A statistical study of the open magnetic flux content of the magnetosphere at the time of substorm onset

P. D. Boakes,[1,2] S. E. Milan,[1] G. A. Abel,[2] M. P. Freeman,[2] G. Chisham,[2] and B. Hubert[3]

[1]   In this paper we determine the probability of substorm onset as a function of open magnetic flux in the magnetosphere by comparing the occurrence distribution of open flux observed at all times with that observed at the time of substorm onset. The open magnetic flux is measured in 12735 auroral images of the ionospheric polar cap from the IMAGE WIC detector. The probability of substorm onset is found to be negligible for fluxes below $\sim$0.3 GWb, increases almost linearly until $\sim$0.9 GWb, and is undefined above this. We also demonstrate that those substorms which show a clear particle injection signature at geosynchronous orbit, as measured by the LANL spacecraft, occur, on average, with higher values of open flux than those showing no activity. We discuss these results in the context of various hypotheses for substorm onset. **Citation:** Boakes, P. D., S. E. Milan, G. A. Abel, M. P. Freeman, G. Chisham, and B. Hubert (2009), A statistical study of the open magnetic flux content of the magnetosphere at the time of substorm onset, *Geophys. Res. Lett.*, *36*, L04105, doi:10.1029/2008GL037059.

1.   Introduction

[2]   There is a general consensus that a necessary condition for substorm onset is the preloading of the magnetosphere with magnetic energy or open magnetic flux [*McPherron*, 1970] but it is unknown how the probability of substorm onset depends on the amount of open flux, and whether this is the only factor determining onset.

[3]   *Kamide et al.* [1977] studied the probability of substorm onset as a function of the latitude of the equatorward boundary of the nightside auroral oval, which is at best indirectly related to the open flux [e.g., *Coumans et al.*, 2007]. They showed there to be a maximum oval latitude above which substorm onsets never occur and a corresponding minimum latitude above which the cumulative probability of onset is 100%. Similarly *Nakai and Kamide* [2004] showed that substorm onset occurs in the upper quartile of the distribution of magnetotail pressure, and *Shukhtina et al.* [2005] found that the total magnetic flux (open and closed) in the magnetotail at substorm onset exceeds 0.8 GWb and is proportional to the magnetopause merging electric field over the preceding hour. Some statistical studies have measured the open flux directly [*Coumans et al.*, 2007; *DeJong et al.*, 2007; *Milan et al.*,

2007]. These reported that open flux varies between $\sim$0.3 and 1.1 GWb at substorm onset but did not show the distribution of these values, which is necessary to determine how the probability of substorm onset varies with this flux.

[4]   In this paper we directly measure the open magnetic flux content of the magnetosphere from a sufficiently large dataset of auroral images to compare the overall distribution of open flux to that at the time of onset, and to determine the probability of substorm onset as a function of open flux for the first time. In section 2 we set out the methodology used to quantify the open flux from auroral images of the ionospheric polar caps taken by the Imager for Magnetopause-to-Aurora Global Exploration (IMAGE) spacecraft, and discuss how we select our data set and sub-categorize our substorms into three categories based on their particle injection signatures. We present our results in section 3 and discuss our findings in section 4.

2.   Method

2.1.   Calculating the Open Magnetic Flux Content of the Magnetosphere

[5]   We estimate the hemispheric open magnetic flux content of the magnetosphere by determining the integral of the radial component of an assumed dipolar magnetic field through the area of the polar cap, which we take to be the dim region encircled by the auroral oval. The open/closed field line boundary (OCB) is then the poleward edge of the oval luminosity region. To determine this hemispheric polar cap flux (F_{pc}) we must be able to determine the latitude of the OCB at all MLTs.

[6]   The latitude of the OCB is estimated from auroral images taken by the Wideband Imaging Camera (WIC) onboard the IMAGE satellite, using the N2 Lyman-Birge-Hopfield band and atomic NI lines (140–180 nm) [*Mende et al.*, 2000]. *Boakes et al.* [2008] have shown that WIC gives at least as good a global proxy for the OCB as either of the Spectrographic Imagers on board the IMAGE spacecraft. WIC also offers better spatial resolution ($\sim$50 km at apogee). In this study we use auroral images from the northern hemisphere from December 2000 and December and January of 2001 and 2002. December and January were used due to the reduced levels of dayglow in these months. Images are available every 2 minutes during 10 hours of each 14 hour orbit. Hence our primary dataset consists of some 77,000 images.

[7]   To identify the OCB we employ the method of *Boakes et al.* [2008], which is explained briefly as follows: Each auroral image is divided into 24 latitudinal profiles, each 1 hour of MLT wide. The latitudinal variation of the longitudinally-averaged intensity within each profile is

---

[1]Department of Physics and Astronomy, University of Leicester, Leicester, UK.
[2]British Antarctic Survey, Cambridge, UK.
[3]Laboratory of Planetary and Atmospheric Physics, University of Liege, Liege, Belgium.
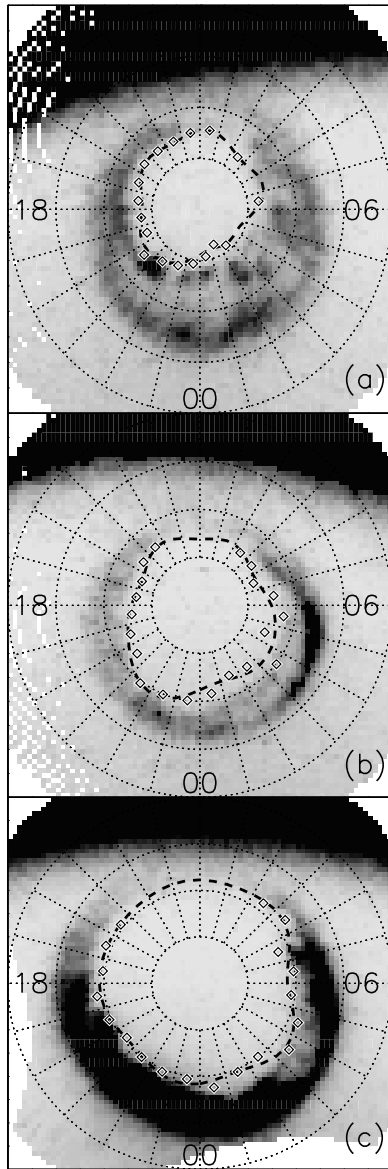
Figure 1. Auroral images from the IMAGE WIC FUV detector for three different values of open flux, (a) 13th January 2002 08:54:41 UT, F_{pc} = 0.36 GWb, (b) 26th December 2001 02:02:07 UT, F_{pc} = 0.57 GWb, (c) 23rd December 2000 04:49:49 UT, F_{pc} = 0.97 GWb. Diamonds represent the OCB estimates at 1 MLT intervals with the thick dashed line showing the final global OCB estimate. Local noon is located at the top of the plots with dotted lines representing lines of constant MLT at 1 MLT intervals. Concentric dotted circles represent lines of constant magnetic latitude at 10° intervals centered on 90°. The dark region at the top of the plots is the result of dayglow swamping the auroral imager.

fitted by a Gaussian plus quadratic function. Here, the Gaussian is expected to fit to the latitudinal profile of the auroral oval, whereas the quadratic fits to any background luminosity, including dayglow. The fit is accepted if the criteria given by *Boakes et al.* [2008] are met. The auroral oval intensity often displays a double Gaussian-like feature with more than one peak in intensity. Thus extra criteria are employed to search for the most poleward peak in auroral intensity. If a fit is accepted the OCB is then assumed to be displaced poleward of the centre of the Gaussian by the full-width-at-half-maximum. We then correct these boundary estimations by applying the systematic offsets found between DMSP particle precipitation boundaries (thought to be the best proxy for the OCB) and IMAGE WIC boundary estimations by *Boakes et al.* [2008, Figure 5].

[8] Figure 1 shows three examples of auroral images from WIC with differing values of F_{pc}. The positions of the OCB estimated in each hour of MLT are shown by diamonds. Visual inspection appears to show that this method gives a good estimate of the expected OCB latitude at most MLTs. However this is not always the case, as seen, for instance, at 04–05 MLT in Figure 1b. Here the OCB estimation has been placed at a higher latitude than its position as suggested by eye. Also, several boundaries may fail the fitting conditions of *Boakes et al.* [2008] resulting in no boundary estimation, for example as seen between 10–15 MLT in Figure 1c. Linear interpolation is used to provide an estimate of the OCB in such cases. However, if the boundary estimation fails in more than six MLT sectors we reject the image (approximately 5/6 of the available auroral images are rejected in this way). In order to smooth out the poor estimations and increase the statistical reliability of the OCB estimates we apply a truncated six-point Fourier Transform, equivalent to a least squares fit of a sixth order Fourier series [*Hamming*, 1989], to the boundary estimations to give the final global estimation of the OCB, shown by the thick dashed line in Figures 1a–1c.

[9] To calculate F_{pc} for each image, we numerically integrate the radial component of an assumed dipolar magnetic field along 48 latitudinal meridians, each a half hour of MLT in width, in steps of 0.5° of latitude from the magnetic pole to the OCB latitude. It is difficult to estimate the uncertainty in the flux calculation, but, as an extreme example, if we assumed the latitude of the OCB at all MLTs to be systematically under or over estimated by 1° then this would lead to an increase or decrease of open flux of about ±10% [*Milan et al.*, 2003].

2.2. Selection of Parent and Substorm Distributions

[10] Applying the above method to all WIC auroral images from December 2000 and December and January of 2001 and 2002 returns an estimate of F_{pc} from 12731 auroral images, the occurrence distribution of which we shall hereafter call the parent distribution.

[11] Using the list of substorm onsets compiled by *Frey et al.* [2004], we find the subset of F_{pc} occurring at the time of substorm onset, the occurrence distribution of which we hereafter call the substorm distribution. Frey et al. identified onsets from auroral images taken by the IMAGE FUV detectors using the following criteria: (1) a clear local brightening of the auroral oval must be observed, (2) the local brightening must expand to the poleward boundary of the auroral oval and spread azimuthally in local time for at least 20 minutes, (3) a substorm onset was only accepted as a separate substorm if at least 30 minutes had passed since the previous onset.

[12] *Frey et al.* [2004] used WIC data in preference to the SI-12/13 data due to its greater spatial resolution. When WIC data were absent SI-13 images were used instead. We
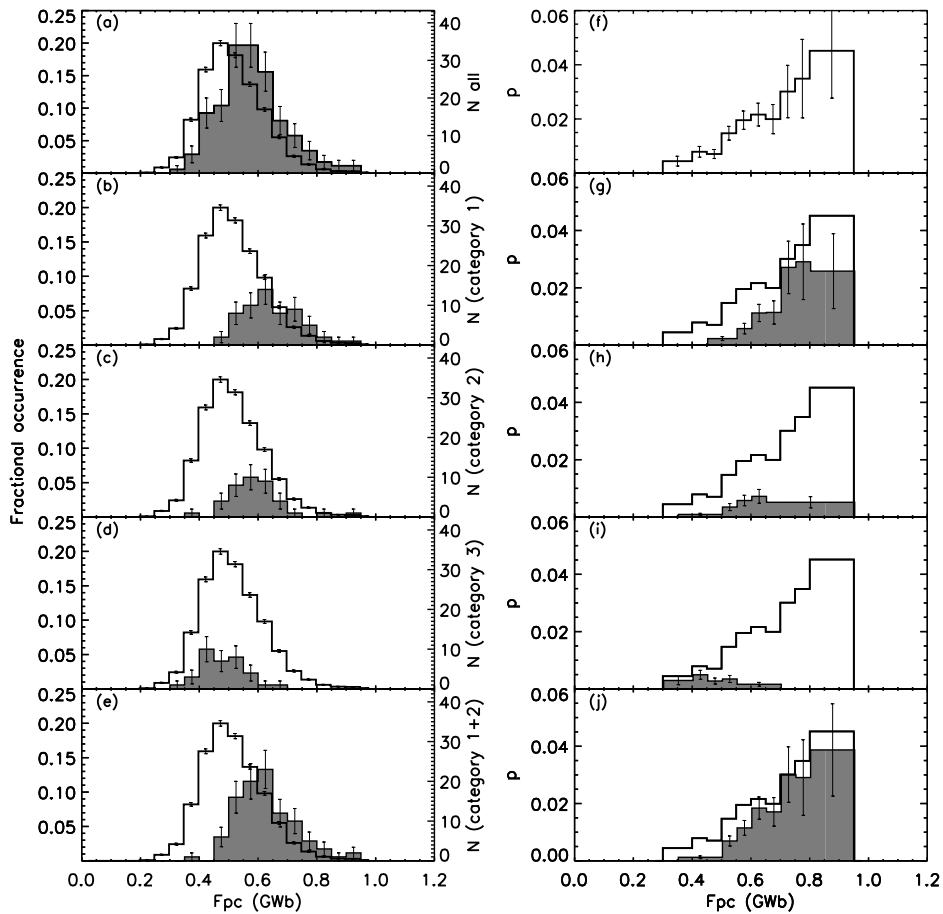
Figure 2. Fractional occurrence, left axis, of parent distribution of open flux (unfilled histogram in all panels) and for (a) all substorms, (b) category 1, (c) category 2, (d) category 3 and (e) category 1&2 (shaded histograms). The right hand axis shows the number in each bin for the relevant substorm distribution. Probability of substorm onset as a function of open flux for (f) all substorms (unfilled histogram repeated in all panels), (g) category 1, (h) category 2, (i) category 3 and (j) category 1&2 substorms (shaded histograms). Error bars are calculated from $\sqrt{N}$ errors. Note that of the 173 substorms in the distribution of Figures 2a and 2f we are able to sub-categorise 145 into categories 1, 2 and 3. Consequently the sum of the shaded probability distribution in Figures 2g–2i does not equal the unshaded probability distribution in Figure 2f.

are unable to determine F_{pc} for many of the images at onset due to a failure to determine the latitude of the OCB in a sufficient number of MLT bins. Thus to increase the size of the substorm distribution, we take the average of F_{pc} from all available values within 4 minutes of every onset time. This results in a substorm distribution containing 173 estimates of F_{pc}. Note that these averaged estimates include those times when an open flux estimate has been made at the onset time. Comparing averaged and unaveraged estimates, we find that the averaging process adds an additional uncertainty on estimates of F_{pc} of ~ 0.03 GWb.

2.3. LANL Substorm Classification

[13] Another signature of substorm onset is the enhancement of energetic particle fluxes at geosynchronous orbit. Energetic particle measurements from the Synchronous Orbit Particle Analyzer (SOPA) onboard the Los Alamos National Laboratory (LANL) satellites [*Belian et al.*, 1992] are used in this study to classify substorms into three categories depending on the particle injection signatures, similar to the criteria used by *Abel et al.* [2006] (examples of which are shown therein): (1). 'classical' substorm injection signature, (2) unclear activity, (3) no activity.

[14] Substorms falling in category 1 will normally have a clear dispersionless enhancement in the midnight sector, followed by dispersed enhancements seen in other satellites (typically two or more) at other local times [*Belian et al.*, 1978; *Baker et al.*, 1979]. Events when no satellite data is available in the midnight sector but a dispersed signature is seen by at least three other satellites, consistent with gradient-curvature drift from a dispersionless enhancement at midnight, are also included in this category. Category 2 covers all other energetic particle fluctuations not falling within category 1. Category 3 events show no fluctuations in any of the LANL spacecraft. To be included in this category data must be available in the midnight sector. Both electron and proton data are used in the classification process.

3. Results

3.1. Open Magnetic Flux at the Time of Substorm Onset

[15] The parent probability distribution of open flux $p(F_{pc})$ is shown by the unfilled histograms in Figures 2a–2e. The substorm probability distribution, $p(F_s) = p(F_{pc}|s)$, is

shown by the shaded histogram in Figure 2a. The open flux of the parent distribution is seen to vary between ∼0.2 and 0.9 GWb with a mean value of $\overline{F}_{pc} = 0.52$ GWb. The open flux at substorm onset varies between 0.3 and 0.9 GWb with a mean value of $\overline{F}_s = 0.58$ GWb. Applying the Kolmogorov-Smirnov (K-S) statistical test to the two distributions verifies that the probability of rejecting the null hypothesis that the two distributions are the same is greater than 0.999.

[16] The shaded histograms in Figures 2b–2e show the distributions of open flux for category 1, 2, 3 and category 1&2 substorms respectively, determined from the LANL spacecraft as defined above. We combine categories 1 and 2 so as to include all possible onset signatures. Of the 173 substorm onsets in the total substorm distribution, 135 have available LANL spacecraft data. Of these, 61 (45%) fall within category 1, 39 (29%) fall in category 2 and 35 (26%) fall in category 3. Substorms occurring in categories 1 and 2 tend to occur at higher values of F_{pc} than those occurring in category 3, with all three categories being significantly different from one another, and from the parent distribution, according to the K-S test. The mean values of F_{pc} for the different substorm categories are as follows; $\overline{F}_1 = 0.66$ GWb, $\overline{F}_2 = 0.59$ GWb, $\overline{F}_{1\&2} = 0.63$ GWb and $\overline{F}_3 = 0.48$ GWb.

3.2. Probability of Substorm Onset as a Function of Open Magnetic Flux

[17] From Bayes' theorem, the probability $p(s|F_{pc})$ of substorm onset occurring in an image at a given value of open flux can be derived from the probability distributions shown in Figures 2a–2e according to

$$p(s|F_{pc}) = \frac{p(s)p(F_s)}{p(F_{pc})} = \frac{n(F_s)}{n(F_{pc})}$$

where n denotes occurrence frequency. Figure 2f shows the function $p(s|F_{pc})$ derived from the parent and all-substorm frequency distributions shown in Figure 2a and is repeated in panels g to j by the unshaded histograms. Similarly, the shaded histograms in Figures 2g–2j show $p(s|F_{pc})$ for the substorm categories shown in Figures 2b–2e. In all cases we have used bins of 0.05 GWb and combined bins in which there are less than 5 events occurring. For all substorms, and for category 1&2, the probability of substorm onset is negligible for fluxes below ∼0.3 GWb, increases almost linearly until $F_{pc} \sim 0.9$ GWb, and is undefined above 0.9 GWb, as fluxes are not observed in this study with values that exceed this.

4. Discussion and Conclusions
4.1. Are All Frey Substorm Events Substorms?

[18] In this study we use substorm onset times derived by *Frey et al.* [2004] from nightside auroral brightenings in IMAGE FUV observations. It is well known that other magnetospheric phenomena can cause auroral brightenings similar to those seen at the time of substorm onset and it is not unlikely that a number of these may have been erroneously included in their substorm list. Therefore, as a secondary indicator of substorm onset we looked for energetic particle injections measured by the LANL spacecraft,

subdividing the substorm distribution into three categories based on these signatures. We found that a significant number of substorms fall into each of the three categories, and showed that the mean of F_{pc} decreases as the injection signature becomes less obvious (see Figures 2b–2d).

[19] One interpretation of this result is that the probability of energetic particles reaching, or being generated at, geostationary orbit following substorm onset decreases for smaller values of F_{pc}. Indeed it has been shown that substorms occurring with contracted polar caps (corresponding to smaller open fluxes) are statistically less energetic than substorms occurring with larger auroral ovals [*Akasofu*, 1975; *Milan et al.*, 2008, 2009]. Furthermore, substorms occurring with lower values of F_{pc}, corresponding to higher onset latitudes, are more likely to map to injection regions significantly tailward of 6.6 R_E.

[20] An alternative view of these results is that category 1 events are almost certainly substorms, with category 2 including both substorm events as well as other phenomena which cause auroral brightenings such as pseudo-breakups or solar wind pressure enhancements. Events falling into category 3 may not be substorms.

4.2. What Do the Distributions Tell Us About Substorm Onset?

[21] We have shown that the occurrence distribution of F_{pc} in the magnetosphere varies between 0.2 and 0.9 GWb, with a mean of 0.52 GWb, in good agreement with the values found by *Milan et al.* [2007, 2008]. The occurrence distribution of F_{pc} at substorm onset also varies between values consistent with those found by *Milan et al.* [2007] and *Coumans et al.* [2007] and occurs with a significantly higher mean (0.59 GWb) than the parent distribution. No substorm onsets are seen to occur below a minimum of 0.3 GWb, showing that the magnetosphere must be preloaded with open magnetic flux as a requirement for substorm onset. If category 1 is considered to be the true substorm distribution then a minimum threshold of 0.4 GWb must be reached before substorm onset is induced, more strongly supporting this view.

[22] *Freeman and Morley* [2004] developed a theoretical model in which the occurrence distribution of substorm onsets, and the distribution of substorm magnitudes [*Morley et al.*, 2007], could be reproduced if substorm onset only depended on a fixed critical threshold in the open magnetic flux. If this were so then we would expect the probability distribution of F_{pc} at substorm onset to be a delta function centered on the threshold value and a sharp cutoff in the parent distribution of F_{pc} at this value. However, Figures 2a–2j do not show this. For all substorm categories, onset can occur over a range of open fluxes (confirming results found by other smaller statistical studies) with the parent distribution extending over this entire range. Here we must also consider whether the distributions can be consistent with a fixed threshold within measurement errors. Using the extreme example of an uncertainty in the open magnetic flux of ∼10%, this gives a maximum error in open magnetic flux of ∼0.1 GWb, much smaller than the spread seen in our distributions.

[23] Whilst most studies agree that the preloading of the magnetosphere is required for substorm onset, others suggest that a further condition must also exist, such as a solar

wind trigger (e.g. a northward turning of the IMF B$_z$) [*Lyons et al.*, 1997; *Hsu and McPherron*, 2002, 2003] (but see also *Henderson et al.* [1996] and *Morley and Freeman* [2007]). If we assume that a solar wind trigger is required to trigger onset once some minimal open magnetic flux threshold has been reached, that triggers occur uniformly randomly with time, and that the open flux increases linearly until a trigger occurs, then we would expect the probability of substorm onset as a function of open flux to show a step function from zero probability of onset below the minimal flux threshold and a decreasing (geometric) distribution above this. This is not seen in our distribution. In fact we may expect the probability to decrease even faster than this because *Hsu and McPherron* [2002] showed that triggers are not uniformly distributed, such that the longer it has been since the last southward turning of the IMF B$_z$, the longer the time expected until a northward turning. Thus a simple model of flux accumulation followed by the triggering of substorm onset by a northward turning of the IMF, where the triggers are either independent or distributed as found by *Hsu and McPherron* [2002], cannot explain the results presented in this paper. The distributions shown in Figure 2 provide constraints on any similar model of substorm onset.

[24] In this study we have concentrated on the relationship of substorm onset to the amount of open magnetic flux in the magnetosphere. However, it may be that there exists another quantity for which a fixed threshold is a necessary and sufficient condition for substorm onset (e.g., the Kappa parameter [*Büchner and Zelenyi*, 1987]) and that the relationship between this and open flux is multi-valued. That is, various configurations of open flux could exist for a given critical value of this quantity. What magnetospheric property this quantity may be is still a matter of speculation and enquiry.

References

Abel, G. A., M. P. Freeman, A. J. Smith, and G. D. Reeves (2006), Association of substorm chorus events with drift echoes, *J. Geophys. Res.*, *111*, A11220, doi:10.1029/2006JA011860.

Akasofu, S. I. (1975), Roles of north-south component of interplanetary magnetic-field on large-scale auroral dynamics observed by DMSP satellite, *Planet. Space Sci.*, *23*, 1349–1354.

Baker, D. N., R. D. Belian, P. R. Higbie, and E. W. Hones (1979), High-energy magnetospheric protons and their dependence on geomagnetic and inter-planetary conditions, *J. Geophys. Res.*, *84*, 7138–7154.

Belian, R. D., D. N. Baker, P. R. Higbie, and E. W. Hones (1978), High-resolution energetic particle measurements at 6.6-R$_E$: 2. High-energy proton drift echoes, *J. Geophys. Res.*, *83*, 4857–4862.

Belian, R. D., G. R. Gisler, T. Cayton, and R. Christensen (1992), High-Z energetic particles at geosynchronous orbit during the great solar proton event series of October 1989, *J. Geophys. Res.*, *97*, 16,897–16,906.

Boakes, P. D., S. E. Milan, G. A. Abel, M. P. Freeman, G. Chisham, B. Hubert, and T. Sotirelis (2008), On the use of IMAGE FUV for estimating the latitude of the open/closed magnetic field line boundary in the ionosphere, *Ann. Geophys.*, *26*, 2759–2769.

Büchner, J., and L. M. Zelenyi (1987), Chaotization of the electron motion as the cause of an internal magnetotail instability and substorm onset, *J. Geophys. Res.*, *92*, 13,456–13,466.

Coumans, V., C. Blockx, J.-C. Gérard, B. Hubert, and M. Connors (2007), Global morphology of substorm growth phases observed by the IMAGE-SI12 imager, *J. Geophys. Res.*, *112*, A11211, doi:10.1029/2007JA012329.

DeJong, A. D., X. Cai, R. C. Clauer, and J. F. Spann (2007), Aurora and open magnetic flux during isolated substorms, sawteeth, and SMC events, *Ann. Geophys.*, *25*, 1865–1876.

Freeman, M. P., and S. K. Morley (2004), A minimal substorm model that explains the observed statistical distribution of times between substorms, *Geophys. Res. Lett.*, *31*, L12807, doi:10.1029/2004GL019989.

Frey, H. U., S. B. Mende, V. Angelopoulos, and E. F. Donovan (2004), Substorm onset observations by IMAGE-FUV, *J. Geophys. Res.*, *109*, A10304, doi:10.1029/2004JA010607.

Hamming, R. W. (1989), *Digital Filters*, 3rd ed., Prentice Hall, Hertfordshire, U. K.

Henderson, M. G., G. D. Reeves, R. D. Belian, and J. S. Murphree (1996), Observations of magnetospheric substorms occurring with no apparent solar wind IMF trigger, *J. Geophys. Res.*, *101*, 10,773–10,791.

Hsu, T.-S., and R. L. McPherron (2002), An evaluation of the statistical significance of the association between northward turnings of the interplanetary magnetic field and substorm expansion onsets, *J. Geophys. Res.*, *107*(A11), 1398, doi:10.1029/2000JA000125.

Hsu, T.-S., and R. L. McPherron (2003), Occurrence frequencies of IMF triggered and nontriggered substorms, *J. Geophys. Res.*, *108*(A7), 1307, doi:10.1029/2002JA009442.

Kamide, Y., P. D. Perreault, S. I. Akasofu, and J. D. Winningham (1977), Dependence of substorm occurrence probability on interplanetary magnetic field and on size of auroral oval, *J. Geophys. Res.*, *82*, 5521–5528.

Lyons, L. R., G. T. Blanchard, J. C. Samson, R. P. Lepping, T. Yamamoto, and T. Moretto (1997), Coordinated observations demonstrating external substorm triggering, *J. Geophys. Res.*, *102*, 27,039–27,051.

McPherron, R. L. (1970), Growth phase of magnetospheric substorms, *J. Geophys. Res.*, *75*, 5592–5599.

Mende, S. B., et al. (2000), Far ultraviolet imaging from the IMAGE spacecraft. 2. Wideband FUV imaging, *Space Sci. Rev.*, *91*, 271–285.

Milan, S. E., M. Lester, S. W. H. Cowley, K. Oksavik, M. Brittnacher, R. A. Greenwald, G. Sofko, and J. P. Villain (2003), Variations in the polar cap area during two substorm cycles, *Ann. Geophys.*, *21*, 1121–1140.

Milan, S. E., G. Provan, and B. Hubert (2007), Magnetic flux transport in the Dungey cycle: A survey of dayside and nightside reconnection rates, *J. Geophys. Res.*, *112*, A01209, doi:10.1029/2006JA011642.

Milan, S. E., P. D. Boakes, and B. Hubert (2008), Response of the expanding/contracting polar cap to weak and strong solar wind driving: Implications for substorm onset, *J. Geophys. Res.*, *113*, A09215, doi:10.1029/2008JA013340.

Milan, S. E., A. Grocott, C. Forsyth, S. M. Imber, P. D. Boakes, and B. Hubert (2009), A superposed epoch analysis of auroral evolution during substorm growth, onset and recovery: Open magnetic flux control of substorm intensity, *Ann. Geophys.*, in press.

Morley, S. K., and M. P. Freeman (2007), On the association between northward turnings of the interplanetary magnetic field and substorm onsets, *Geophys. Res. Lett.*, *34*, L08104, doi:10.1029/2006GL028891.

Morley, S. K., M. P. Freeman, and E. I. Tanskanen (2007), A comparison of the probability distribution of observed substorm magnitude with that predicted by a minimal substorm model, *Ann. Geophys.*, *25*, 2427–2437.

Nakai, H., and Y. Kamide (2004), A critical condition in magnetotail pressure for leading to a substorm expansion onset: Geotail's observations, *J. Geophys. Res.*, *109*, A01205, doi:10.1029/2003JA010070.

Shukhtina, M. A., N. P. Dmitrieva, N. G. Popova, V. A. Sergeev, A. G. Yahnin, and I. V. Despirak (2005), Observational evidence of the loading-unloading substorm scheme, *Geophys. Res. Lett.*, *32*, L17107, doi:10.1029/2005GL023779.

_____

G. A. Abel, G. Chisham, and M. P. Freeman, British Antarctic Survey, Cambridge CB3 0ET, UK.

P. D. Boakes and S. E. Milan, Department of Physics and Astronomy, University of Leicester, Leicester LE1 7RH, UK. (p.boakes@ion.le.ac.uk)

B. Hubert, Laboratory of Planetary and Atmospheric Physics, University of Liege, B-4000 Liege, Belgium.